ADAPTIVE FILTERED-BACK-PROJECTION FOR COMPUTED TOMOGRAPHY

Joseph Shtok, Michael Elad, and Michael Zibulevsky

The CS Department – The Technion, Haifa 32000, Israel

ABSTRACT

We propose an extension of the Filtered Back-Projection (FBP) algorithm for reconstruction of attenuation images in Computed Tomography (CT). In our scheme, the standard filtering of projections with windowed ramp kernel is replaced by an adaptive, spatially-variant linear filter, based on a structured bank of 2D convolution kernels. In addition, the proposed scheme includes a post-processing step of image filtering by convolution with a 2D adaptive filter. Both filters are trained for specified reconstruction task via an optimization of corresponding objective function. The reconstruction task is defined through (i) a representative set of specific family of images; (ii) data acquisition conditions (partial set of projections, noise level); and (iii) a Region-Of-Interest (ROI) to be recovered. The resulting adaptive scheme absorbs various imperfections of reconstruction algorithm and specializes to given task, effectively improving the reconstruction quality.

Index Terms— Computed Tomography, truncated projections, adaptive scheme, trained filter.

1. INTRODUCTION

In transmission tomography, FBP is the main direct algorithm employed for CT reconstruction in 2D parallel-beam scanning geometry. It is simple, fast, and theoretically precise, implementing the Radon inversion formula for X-ray transform in two dimensions. In practice, FBP has a number of serious drawbacks, among which, this algorithm is oblivious of the statistical data acquisition model, hence has very limited adaptivity to given reconstruction task. A number of improvements has been made in the reconstruction scheme, achieving better performance and reducing artifacts – pre-processing of the projections set, smart discretization and interpolation operators, post-processing of the images, and more. Despite that, the core component of FBP - projections filter - remains almost unchanged.

Despite low reconstruction quality, usage of FBP has its merits. More elaborate, statistically based algorithms provide better performance but at the cost of increased computation time, since they require iterative computations with huge data volumes. Time is often a critical factor in clinical radiology, especially in computer-aided surgery. It is therefore important to improve direct reconstruction algorithms.

Our approach to the task of reconstruction from ill-conditioned data consists of extending the formally derived FBP algorithm to a robust adaptive scheme using a statistically based training process. In practical reconstruction, our scheme should compensate for discretization errors, present noise characteristics, incompatibility of the projection transform (realized in CT hardware) and the back-projection (implemented in software). Also, the desired family of images and data acquisition conditions are taken into account, specializing the algorithm to local requirements. An important benefit of our approach is the fact that the new reconstruction algorithm relies on the existing FBP core, and as such, requires minor modifications in existing CT reconstruction tools. Numerical experiments display the advantage of this scheme over the standard FBP algorithm.

This paper is organized as follows: Section 2 provides background material and brief survey of related work. In Section 3 we define the filtering design goal, and the proposed reconstruction scheme architecture. The focus of Section 4 is the kernel design itself, and experiments are reported in Section 5.

2. PROBLEM STATEMENT AND BACKGROUND

We now introduce the problem setup and terminology of 2D computed tomography. For a broad introduction to the subject, the reader is referred to [3, 7, 10]. Let $\mu(x_1, x_2)$ be a two-dimensional attenuation image. The scan data, obtained in parallel beam scanning geometry, comprises of a set of measurements $\{y_\ell\}$, for some collection of lines $\ell = \ell(\theta, s)$ in the plane, parameterized by the angle θ between the line and the x axis, and by the distance s of the line from the origin. To account for photon counting errors, the measurements y_ℓ are modeled as realizations of random variables $y_\ell \sim \text{Poisson}\left(I_0 e^{-(\mathbf{R}f)_\ell}\right)$, where $(\mathbf{R}f)_\ell = \int_\ell \mu(x_1, x_2) dl$ is the Radon transform of μ at line ℓ and I_0 is X-ray intensity of the source. This is a simplified statistical model for transmission tomography scan, which can be extended to account for many physical phenomena [12]. As seen, the variance of the resulting Poisson noise depends on the initial X-ray intensity as well as on the scanned object.

A set of projections (sinogram) is obtained from the measurements $\{y_\ell\}$ by $g_\theta(s) = -\log \frac{y_{\ell(\theta,s)}}{I_0}$. In the noiseless

case ($y_\ell = I_0 e^{-(\mathbf{R}f)_\ell}$), we have simply $g = \mathbf{R}f$. Filtered-Back-Projection is a direct algorithm for reconstruction of the attenuation function $\mu(x_1, x_2)$ from the sinogram $g_\theta(s)$. It is based on the Radon inversion formula, and consists of two steps: (i) Apply a convolution filter to each projection g_θ, with the kernel $\kappa(t)$ defined in Fourier domain by $\hat{\kappa}(\omega) = |\omega|$ (the filter of Ramachandran and Lakshminarayanan (Ram-Lak), also known as the ramp filter [11]); and (ii) Apply the adjoint $\mathbf{R}^*$ of the Radon transform (the back-projection transform).

In continuous domains, with noiseless data and an ideal projection and back-projection pair, the above algorithm is exact. However, real-world applications suffer from various problems: (i) The kernel $\kappa(t)$ amplifies the high-frequency noise; (ii) CT scanner does not produce an exact Radon transform, and the back-projection transform implemented in software may not accurately represent its adjoint; (iii) Discretization errors are introduced in both stages of the algorithm; and (iv) The global nature of the two-dimensional Radon transform does not allow to apply FBP to partial projection data (e.g., a set of projections through a Region-Of-Interest, limited or sparse angles, or a partial field of view).

There are various techniques proposed for addressing these problems. We briefly mention few such attempts. As to the filter to apply, it has been observed that a proper filter design can improve the reconstruction [4, 8]. Windowing of filter kernel in the Fourier domain to the desired bandwidth helps to eliminate the high frequency noise. Hann or Butterworth windows are usually applied to the ramp kernel, or a Shepp-Logan kernel is used, which has properties similar to the windowed ramp filter. Non-linear filtering is also proposed [1]. A sinogram correction before the application of FBP is also considered and practiced for improved reconstruction [12, 9]. In [12], the sinogram is restored by iteratively optimizing a statistically based penalty function.

In [6] B-spline decomposition is used to construct an effective implementation of Radon transform and the FBP, with reduced interpolation and discretization errors. Accurate statistical modeling of the acquisition process provides high-quality reconstruction images obtained as the optimizer of a Penalized Likelihood (PL) function. It is computed iteratively using wide range of specially designed optimization techniques. Desired properties of a reconstructed image can be introduced to PL function as a prior, thus improving the quality of reconstruction. We refer to the papers [5, 2] for comprehensive description of such algorithms.

3. ADAPTIVE FBP ALGORITHM

3.1. General

We propose an extension of the FBP algorithm, called Adaptive-FBP (AFBP), which employs more powerful and robust filtering stages, combined with adaptive filter design. The kernel bank for AFBP filters is trained for a reconstruction task via an off-line optimization process, with corresponding objective function. The task is defined by the following parameters:

1. The family $\mathcal{F}$ of images, on which the algorithm is to be applied. In medical imaging such specialization is often possible: besides the fact that all clinical tomographic images represent a family with quite special properties (piecewise smooth images consisting of distinct tissues), also scans of individual organs have their common intrinsic properties. We empirically establish a clear gain in reconstruction quality emerging from training the algorithm parameters on a set of such images from a given family.

2. The structure of available set of projections. The projections are allowed to be truncated to a specific ROI, or lack some subset of projection angles, or have some other limitations. While the perfect reconstruction in many such cases is impossible, the algorithm attempts to compensate the missing data by a training process.

3. The X-ray intensity of the scan. It helps determining the variance of the Poisson noise, present in projections (which is also data-dependent).

Basic merits of the proposed scheme are (i) avoiding iterative algorithms; (ii) adapting to the problem characteristics (projection limitations, family of images, noise behavior, model imperfections, and more); and (iii) preserving existing CT devices' configurations, while being able to provide higher quality reconstruction, or reduced X-ray dosage.

3.2. Reconstruction scheme

Since in practice the conditions for precise reconstruction are not met, we abandon the attempt to implement a theoretically exact formula for inverse Radon operator; instead, we use a robust reconstruction scheme, presented below, which parameters are optimized for specified objective function. The reconstruction procedure is defined by the following operator:

$$\mathbf{T}_{\kappa,\nu} : g \xrightarrow{\mathbf{F}^P_\kappa} \hat{g} \xrightarrow{\mathbf{R}^*} f^1 \xrightarrow{\mathbf{F}^I_\nu} \tilde{f}. \tag{1}$$

Here, $\mathbf{F}^P_\kappa$ is a filter operator in the projection domain, applied with a set of parameters κ. Filter structure is detailed below. Similarly, $\mathbf{F}^I_\nu$ is a filter operator in the image domain, which is a 2D convolution with kernel ν. $\mathbf{R}^*$ stands for the back-projection operator, and the resulting $\tilde{f}$ is the estimate for attenuation map. Notice that FBP is the special case of this algorithm, when $\mathbf{F}^P$ acts by a convolution with the ramp kernel and $\mathbf{F}^I = \mathbf{1}$.

Use of adaptive scheme allows us to extend the filter type of $\mathbf{F}^P_\kappa$ from a constant one-dimensional convolution kernel, applied to each projection (as practiced today with FBP), to a

more general linear filter. We consider the following generalizations:

1. **2D convolution kernel:** Despite the fact that the theoretical Radon inversion formula only requires a separate filtering of the sinogram projections, valuable information can in practice be provided by the neighboring projections. Thus we can use a 2D convolution kernel $h(x_1, x_2)$, applied on a neighborhood of each projection g_θ. The single filtered projection $\hat{g}_\theta$ is then extracted from the convolution output.

2. **Angle-dependent convolution kernel:** We aim to compensate for the angular discretization error of the back-projection operator, which accounts differently for projections parallel to x axis of the image grid and for those making an angle of $\pi/4$ rad with the axis. This problem is addressed by *angular differentiation of kernels*, using a different convolution kernel h_θ for each projection angle θ. In practice, the angle-parameterized kernel bank is deployed from a small number of pivot kernels $\{h_{\theta_k}\}$, for angles $\{\theta_k,\ k = 1, ..., K\}$ evenly distributed over over the range $[0, \pi/8]$[1]. The kernels for intermediate angles are computed as weighed linear combinations of the two nearest pivots: for each relevant $0 \le \theta \le \pi/8$ with $\theta_k < \theta < \theta_{k+1}$, we let $h_\theta = (1-\alpha)h_{\theta_k} + \alpha h_{\theta_{k+1}}$, where $\alpha = (\theta - \theta_k)/(\theta_{k+1} - \theta_k)$.

3. **Distance-dependent convolution kernel:** There is a difference between central and peripheral regions of the image, expressed both in the discretization aspects of the sinogram and in properties of attenuation maps. More specifically, a central pixel in the attenuation image generates a curve in the sinogram, which is discretized differently from the curve generated by a peripheral pixel. In the attenuation image, peripheral regions often feature the body boundaries and the blank areas outside the body. Thus, a spatially-variant projection filtering can and should be devised to account for these distinctions. In the first version of *spatial differentiation of kernels*, we train a sequence of kernels κ_s for a number of fixed, unsigned distances s from the center of the image (and of the projection vector). Thus each segment of the projection will be filtered by convolution with corresponding κ_s. Spatially-variant filtering has special importance in case of ROI reconstruction. When the projections are truncated to the region of interest, central part of the remaining projection should be filtered using a symmetric kernel with small spatial support, to reduce the truncation error. For projection pixels which reside near the edges of the region, the information should be gathered in a non-symmetric way, only from non-truncated part of the projection. These considerations entail use of more elaborate spatially-variant filtering, where the kernel bank is parameterized by a signed distance s from the projection center, and the values of s vary from 0 to the radius of ROI. Such design is the second version of spatial differentiation, used in the algorithm.

Filter generalizations ("features") detailed above are mutually independent, hence can be combined into a powerful and flexible sinogram filtering operator with high-dimensional set of parameters. This linear operator treats each pixel in the sinogram according to its angular and radial location, with proper account of its neighborhood and truncation conditions. The key constituent of the AFBP scheme is the way the kernels κ and ν are derived. It is presented in the following section.

[1]This bank of kernels is then mirrored and duplicated to cover the corresponding sectors of the whole scan range

4. KERNELS DESIGN BASED ON RECONSTRUCTION TASK

The basic reconstruction scheme is adjusted to the given reconstruction task. Information defining this task is conveyed to the algorithm through the training of the kernel banks κ, ν, optimized for the appropriate objective function. This information consists of the following items:

- Training set $\mathcal{F}_{tr}$ of high-quality representatives of the desired family of attenuation images.
- Acquisition conditions expressed by a truncation operator $\mathbf{E}_P$ in projection domain, expressing the available projection set
- Reconstruction requirements expressed by a truncation operator $\mathbf{E}_I$ on image domain, which defines the required region for reconstruction.
- X-ray intensity of the scanner, which influences the variance of Poisson noise in measurements.

The training procedure uses $\mathcal{F}_{tr}$ to generate a training set $\mathcal{G}_{tr}$ of noisy sinograms, defined as

$$\mathcal{G}_{tr} = \{g_f^k = \mathbf{E}_P(\mathbf{R}f + \xi_f^k) \mid f \in \mathcal{F}_{tr}, k = 1...K\}, \qquad (2)$$

where $\{g_f^k\}_{k=1}^K$ are generated from the image $f \in \mathcal{F}_{tr}$ by applying the implemented projection transform $\mathbf{R}$ and generating K instances of the Poisson noise, by our model (more elaborate statistical acquisition model can be used here for a real-world algorithm). The filters are then computed as the optimizers of the objective function

$$(\kappa^*, \nu^*) = \arg\min_{\kappa,\nu} \sum_{g_f^k \in \mathcal{G}_{tr}} \|\mathbf{E}_I(\mathbf{T}_{\kappa,\nu} g_f^k - f)\|_2^2. \qquad (3)$$

Since the penalty function is quadratic in each of the kernels κ and ν, we can solve it using the Conjugate Gradient method, applied to the corresponding linear equation representing the derivative of the penalty function. The training of the pair (κ, ν) is then carried out in turns, fixing one kernel and updating the other.

The resulting algorithm improves on FBP in two conceptually different ways: first, use of more elaborate filter type

with rich structure and adaptive properties helps compensating for imperfections of the entire chain of CT acquisition, from detectors to final image. This is plausible since the training stage promotes the similarity of algorithm output to the high-quality images of the training set. These imperfections include the discretization errors, incompatibility between the hardware projector and the implemented back-projector operators, noise introduced at different stages, and more.

Second, the special structure of training set images and the acquisition conditions may require, for the best results, filter kernels quite different from the universal ramp kernel. Notice that when applying the FBP to truncated projections, the quality of reconstruction hinges on the filtering step of the algorithm: the very problem of truncated projection data consists of the incorrect projection filtering. The back-projection, which gathers for each image pixel the values of projections through it, lacks no information for ROI reconstruction. This justifies the expected gain in reconstruction quality, coming from filter training on the truncated data.

Numerical experiments, presented in Section 5, display the influence of various filter extensions on the reconstruction quality and support the considerations for the algorithm design.

5. EMPIRICAL RESULTS

We conduct an experiment of ROI reconstruction from truncated projections. In images of size 128^2, we choose the ROI to be the central disk of radius 20 pixels. Projections are computed through a disk with radius 24 pixels, i.e. we allow a small margin to reduce the edge effects of ROI reconstruction. Training set comprises of 10 clinical CT images, retrieved as 2D slices from a Cone-Beam scan. Similar 18 images constitute the testing set. We use a number of kernel banks types κ in the projection domain, as detailed below. All kernels are of length $\sqrt{2}n$, where n is the projection length:

- $\mathbf{B}\_1\_1\_1$ is a single 1D trained kernel.
- $\mathbf{B}\_5\_1\_1$ is a 2D kernel with dimensions $\sqrt{2}n \times 5$.
- $\mathbf{B}\_1\_5\_1$ is a bank of 5 1D kernels, which represent the pivots for angular differentiation.
- $\mathbf{B}\_1\_1\_5$ is a bank of 5 1D kernels, which are applied at different signed distances from the projection center.
- $\mathbf{B}\_5\_5\_5$ combines the three previous features: it is a bank of 5 sets of 2D kernels, responsible for different projection pivot angles. Each set comprises of 5 kernels, applied at different signed distances from the projection center.

In the image domain the adaptive convolution kernel used is a square matrix of size 21×21.

We compare our algorithms with FBP applied with a classical windowed ramp filter. The frequency cut-off and the degree of window are tuned to the best performance on the training set.

The results display begins with the training set, where performance of different kernel banks compares clearly (Figure 1). Single trained kernel $\mathbf{B}\_1\_1\_1$ improves the standard FBP with windowed ramp by 6.74 dB on average[2]. Spatial differentiation raises the average SNR by 0.37 dB more, and all three features used together result in 0.76 dB improvement over the single trained kernel. Usage of 2D kernels or of the angular differentiation alone improves the training set performance by 0.18 or 0.27 dB, respectively[3].

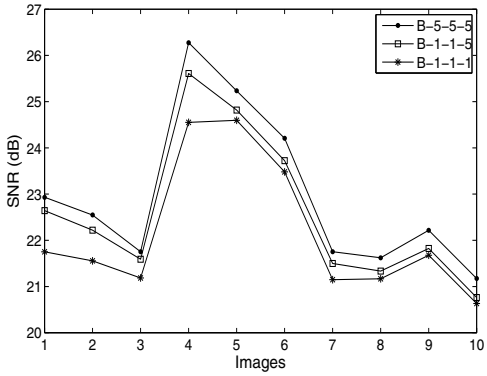

Fig. 1. Performance of AFBP on the training set.

For the testing set (Figure 2), we choose to show the results only for $\mathbf{B}\_1\_1\_1$ and $\mathbf{B}\_5\_5\_5$ among the AFBP versions, since the SNR values for the other kernel banks fall in the narrow range between them. The mean improvement of FBP performance is $6.7 \div 7.0$ dB, for all AFBP kernel banks.

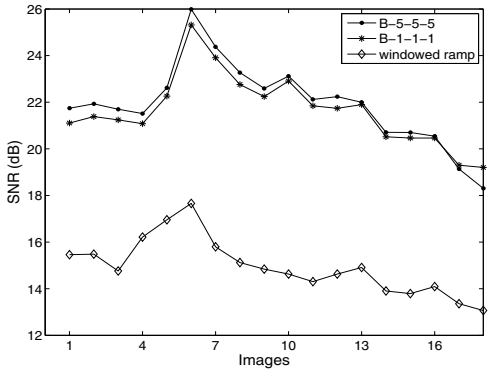

Fig. 2. Performance of AFBP vs. FBP on the testing set.

[2]The plain FBP is not shown in the graph, since it scales-down the axes too much.

[3]The use of 2D kernels does have a notable impact on the algorithm performance in the setup of reconstruction from full projections. Such an experiment is not displayed in this paper due to lack of space.

Finally, we display performance of some chosen algorithms on general set of clinical CT images of thorax, not similar to those which constitute the training set. SNR values presented in Figure 3 show that AFBP outperforms the standard FBP algorithm also beyond the scope of targeted family of attenuation images. On this image set, the mean gain is 3.3 dB Visual comparison of the ROI images and the reconstruction errors is displayed in figure 4.

6. SUMMARY

We have presented an extension of the basic direct algorithm for CT reconstruction - the Filtered Back-projection (FBP). This extension allows to specialize the FBP for various important tasks in Computed Tomography, such as reconstruction of attenuation images of known nature, reconstruction of Region-Of-Interest from partial projection sets, robust treatment of projections noise and other phenomena properly modeled into the objective function of AFBP training. The algorithm is easily implemented and can be effortlessly incorporated in existing scanning devices. A number of algorithms were developed and tested numerically, using Matlab environment.

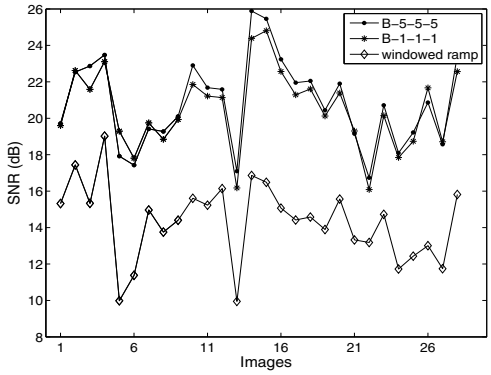

Fig. 3. Performance of AFBP vs. FBP on a general set.

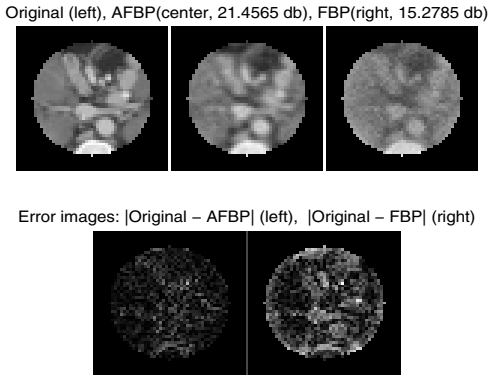

Fig. 4. Visual comparison between AFBP and FBP.

7. REFERENCES

[1] B.I. Anda, K.D. Sauer, and C.A. Bouman, "Nonlinear Back-projection for tomographic reconstruction", *IEEE Trans. on Nuclear Science*, Vol. 49, No. 1, February 2002.

[2] I.A. Elbakri and J.A. Fessler, "Statistical image reconstruction for polyenegretic X-Ray Computed Tomography", *IEEE Trans. on Medical Imaging*, Vol. 21, No. 2, February 2002.

[3] A. Faridani, "Introduction To The Mathematics Of Computed Tomography", *MSRI Publications*, vol. 47, 2003.

[4] T.H. Farquhar, A. Chatziioannou, G. Chinn, M. Dahlbom, and E.J. Hoffman, "An investigation of filter choice for filtered back-projection reconstruction in PET", *IEEE Nuclear Science Symposium*, 1997.

[5] J.A. Fessler, "Penalized weighted least-squares image reconstruction for positron emission tomography", *IEEE Trans. on Medical Imaging*, Vol. 13, No. 2, pp. 290–300, June 1994.

[6] S. Horbelt, M. Liebling, and M. Unser, "Discretization of the Radon transform and of its inverse by spline convolutions", *IEEE Trans. on Medical Imaging*, Vol. 21, No. 4, April 2002.

[7] A.C. Kak, *Principles Of Computerized Tomographic Imaging*, IEEE press, 1999.

[8] J.H. Kim, K.I. Kim, and C.E. Kwark, "A filter design for optimization of lesion detection in SPECT", *IEEE Nuclear Science Symposium*, 1996.

[9] T. Li, X. Li, J. Wang, J. Wen, H. Lu, J. Hsieh, and Z. Liang, "Nonlinear sinogram smoothing for Low-Dose X-Ray CT", *IEEE Trans. on Nuclear Science*, Vol. 51, No. 5, October 2004.

[10] F. Natterer, F. Wubbeling, *Mathematical Methods In Image Reconstruction*, SIAM, 2001.

[11] G.N. Ramachandran and A.V. Lakshminarayanan, "Three-dimensional reconstruction from radiographs and electron micrographs: application of convolutions instead of fourier transforms", *Proceedings Of The National Academy Of Sciences Of The United States Of America*, Vol. 68, No. 9, 1971.

[12] P.J. La-Riviere, J. Bian, and P.A. Vargas, "Penalized-likelihood sinogram restoration for computed tomography", *IEEE Trans. on Medical Imaging*, Vol. 25, No. 8, August 2006.